Published in final edited form as:

Cell Rep. 2016 June 7; 15(10): 2239–2250. doi:10.1016/j.celrep.2016.05.012.

Complexin 3 Increases the Fidelity of Signaling in a Retinal Circuit by Regulating Exocytosis at Ribbon Synapses

Lena S. Mortensen[1,6], **Silvia J.H. Park**[2,6], **Jiang-bin Ke**[3], **Benjamin H. Cooper**[1], **Lei Zhang**[3], **Cordelia Imig**[1], **Siegrid Löwel**[4], **Kerstin Reim**[1], **Nils Brose**[1], **Jonathan B. Demb**[2,5], **Jeong-Seop Rhee**[1,7], and **Joshua H. Singer**[3,*,7]

[1]Department of Molecular Neurobiology, Max Planck Institute of Experimental Medicine, 37075 Göttingen, Germany

[2]Department of Ophthalmology and Visual Science, Yale University, New Haven, CT 06511, USA

[3]Department of Biology, University of Maryland, College Park, MD 20742, USA

[4]Department of Systems Neuroscience, Bernstein Focus Neurotechnology, Johann-Friedrich-Blumenbach Institute for Zoology and Anthropology, University of Göttingen, 37075 Göttingen, Germany

[5]Department of Cellular and Molecular Physiology, Yale University, New Haven, CT 06511, USA

SUMMARY

Complexin (Cplx) proteins modulate the core SNARE complex to regulate exocytosis. To understand the contributions of Cplx to signaling in a well-characterized neural circuit, we investigated how Cplx3, a retina-specific paralog, shapes transmission at rod bipolar (RB) → AII amacrine cell synapses in the mouse retina. Knockout of Cplx3 strongly attenuated fast, phasic Ca^{2+}-dependent transmission, dependent on local [Ca^{2+}] nanodomains, but enhanced slower Ca^{2+}-dependent transmission, dependent on global intraterminal [Ca^{2+}] ($[Ca^{2+}]_I$). Surprisingly, coordinated multivesicular release persisted at $Cplx3^{-/-}$ synapses, although its onset was slowed. Light-dependent signaling at $Cplx3^{-/-}$ RB → AII synapses was sluggish, owing largely to increased asynchronous release at light offset. Consequently, propagation of RB output to retinal ganglion cells was suppressed dramatically. Our study links Cplx3 expression with synapse and circuit function in a specific retinal pathway and reveals a role for asynchronous release in circuit gain control.

*Correspondence: jhsinger@umd.edu.
[6]Co-first author
[7]Co-senior author

SUPPLEMENTAL INFORMATION

Supplemental Information includes Supplemental Experimental Procedures and two figures and can be found with this article online at http://dx.doi.org/10.1016/j.celrep.2016.05.012.

AUTHOR CONTRIBUTIONS

Conceptualization, S.L., K.R., N.B., J.-S.R., and J.H.S.; Funding Acquisition, S.L., N.B., J.-S.R., J.B.D., and J.H.S.; Resources, K.R. and N.B.; Investigation, L.S.M., S.J.H.P., J.-b.K., B.H.C., L.Z., and C.I.; Formal Analysis, L.S.M., S.J.H.P., J.-b.K., B.H.C., L.Z., C.I., J.B.D., J.-S.R., and J.H.S.; Supervision, K.R., N.B., J.B.D., J.-S.R., and J.H.S.; Visualization, L.S.M., B.H.C., J.B.D., and J.H.S.; Writing – Original Draft, L.S.M., J.B.D., and J.H.S.; Writing – Review & Editing, L.S.M., S.J.H.P., B.H.C., K.R., N.B., J.B.D., J.-S.R., and J.H.S.

Graphical abstract

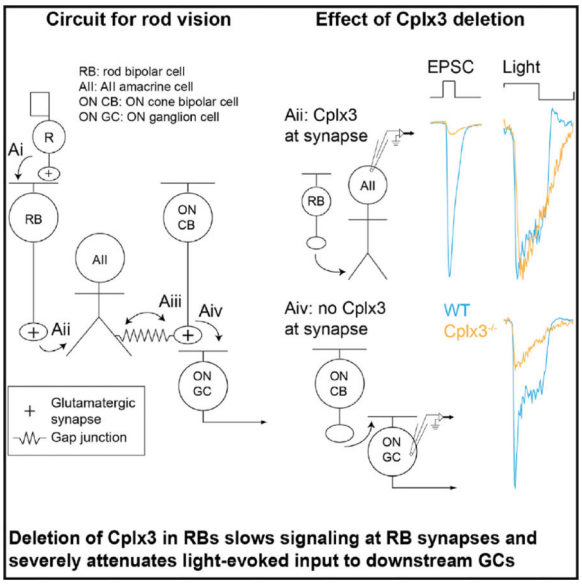

INTRODUCTION

Neural circuit function depends critically on mechanisms that link presynaptic depolarization to the postsynaptic response. A key component of this process is the coupling between presynaptic Ca^{2+} influx and exocytosis (Kaeser and Regehr, 2014; Kavalali, 2015; Rizo and Xu, 2015; Schneggenburger and Rosenmund, 2015). Several proteins alter the Ca^{2+} sensitivity of exocytosis and allow one nerve terminal to sustain multiple modes of transmission, i.e., spontaneous (independent from Ca channel opening), phasic (time locked to presynaptic Ca^{2+} influx), and asynchronous (driven by residual $[Ca^{2+}]_I$ after closure of Ca channels) (Kaeser and Regehr, 2014; Kavalali, 2015; Schneggenburger and Rosenmund, 2015).

Understanding the functions of proteins that modulate exocytosis is critical in assessing contributions of these transmission modes to synaptic signaling. The complexin (Cplx) family of proteins apparently contributes to the diversity of exocytotic modes: Cplxs bind to the core SNARE complex and lower the free-energy barrier to membrane fusion, thereby increasing the efficiency of Ca^{2+}-dependent exocytosis; also, Cplxs might act as brakes on spontaneous fusion to preserve vesicles in a release-ready state (Trimbuch and Rosenmund, 2016).

We assessed the role of the retina-specific isoform Cplx3 in regulating transmitter release from rod bipolar cells (RBs), which serve as a model system for studying ribbon synapses, the specialized synapses of excitatory neurons in primary sensory structures (Matthews and Fuchs, 2010). Paired voltage-clamp recordings from presynaptic RBs and postsynaptic AII amacrine cells (AIIs) reveal multiple release modes—phasic, tonic, asynchronous, and spontaneous—in excitatory postsynaptic currents (EPSCs) recorded in AIIs (Mehta et al., 2014; Singer and Diamond, 2003). Among the known Cplxs, RBs express only Cplx3

(Landgraf et al., 2012; Reim et al., 2009; Vaithianathan et al., 2015), and in mice lacking Cplx3, we reveal the role that Cplx3 plays at RB → AII synapses and the influence that its synaptic function has on light-evoked circuit output to retinal ganglion cells (GCs) (Demb and Singer, 2015).

RESULTS

Loss of Cplx3 from RBs Severely Attenuates Phasic Exocytosis

Localized $[Ca^{2+}]_I$ changes originating from single Ca channel openings ($[Ca^{2+}]_I$ "nanodomains") evoke synchronized, phasic release from RBs (Jarsky et al., 2010). Such $[Ca^{2+}]_I$ changes are small, and nanodomain Ca^{2+} exocytosis coupling suggests that vesicle release at RB active zones (AZs) is triggered by relatively low $[Ca^{2+}]_I$, with an effective dissociation constant, K_D, of the vesicular Ca^{2+} sensor ≈ 10 μM (Jarsky et al., 2010). Because Cplxs facilitate and synchronize evoked neurotransmitter release by stabilizing partially assembled SNARE complexes at conventional synapses (Trimbuch and Rosenmund, 2016), we tested the hypothesis that the high efficiency of the phasic-release process at RB synapses depends on Cplx3.

During paired voltage-clamp recordings, brief voltage steps (5 ms to −10 mV) in RBs evoked large EPSCs in AIIs of wild-type (WT) retinas; as expected, AMPAR-mediated EPSCs exhibited short latencies to onset and fast rise times (Figures 1A and 1B) (Jarsky et al., 2010; Singer and Diamond, 2003). At $Cplx3^{-/-}$ synapses, RB Ca currents (I_{Ca}) were unchanged, but EPSC amplitudes were reduced ~3-fold relative to WT (Figures 1A and 1B). Exocytosis at $Cplx3^{-/-}$ synapses was slowed and desynchronized as evidenced by lengthened latencies and rise times observed in both EPSCs and current integrals (Figures 1B3, 1B4, and 1C). EPSC decay, reflecting AMPAR deactivation (Jarsky et al., 2011; Singer et al., 2004), was unaffected (WT versus $Cplx3^{-/-}$: 3.9 ± 0.2 ms versus 4.2 ± 0.5 ms; $p > 0.05$). As quantal content (QC) of the EPSC evoked by brief presynaptic depolarization approximates the readily releasable pool (RRP) of vesicles at the RB AZ (Singer and Diamond, 2006), to a first approximation, the RRP at $Cplx3^{-/-}$ synapses was reduced. Electron microscopic (EM) analysis of the RB terminal ultrastructure demonstrated that the decreased RRP did not result from a reduced number of ribbon-associated vesicles (Figure S1).

Release latency was examined further using a ramp stimulus that allowed us to correlate the timing of release events with presynaptic membrane potential (V_M) and Ca channel opening (Jarsky et al., 2010). A 1 mV/ms ramp from −60 to −30 mV evoked a transient EPSC followed by desynchronized synaptic currents (Figure 1D); as ramp slope decreased, release became more desynchronized, and the transient EPSC became smaller and ultimately disappeared. Here, "desynchronized" refers to events occurring during the stimulus, whereas "asynchronous" events occur red following the stimulus and the closure of RB Ca channels. Although transient EPSCs were attenuated, or even absent, at $Cplx3^{-/-}$ synapses, desynchronized events persisted (Figure 1D) with amplitudes unchanged (data not shown).

At WT synapses, EPSCs were observed first at RB V_M = −50 mV and I_{Ca} ≈ 3 pA. Assuming a single channel I_{Ca} ≈ 0.15 pA (1.15 mM $[Ca^{2+}]_E$) and Ca channel distribution

over ~55 AZs (Jarsky et al., 2010; Mehta et al., 2014; Tsukamoto and Omi, 2013), ~0.36 Ca channels would be opened at each AZ. Assuming Poisson statistics, the probability of >1 Ca channel opening per AZ ≈ 0.05. Therefore, at the threshold for exocytosis, release of a vesicle depended on a single Ca channel opening and, therefore, was regulated by a $[Ca^{2+}]_I$ nanodomain (Jarsky et al., 2010). At Cplx3$^{-/-}$ synapses, however, EPSCs appeared at V_M = −43 mV (I_{Ca} ≈ 9 pA), and the probability of multiple channel openings per AZ ≈ 0.30.

Thus, Cplx3 deletion disrupts nanodomain control of exocytosis. This could result from either impaired physical Ca channel-release site coupling or altered Ca^{2+} sensitivity of vesicles proximate to Ca channels. To distinguish between these alternatives, intracellular [Bapta] ($[Bapta]_I$) was reduced from 1 to 0.1 mM. Were vesicles at Cplx3$^{-/-}$ AZs farther from Ca channels, lowered $[Bapta]_I$ should have restored phasic release by permitting free Ca^{2+} to diffuse farther from its site of entry, but it did not: EPSC amplitudes and waveforms at WT and Cplx3$^{-/-}$ synapses were unchanged (data not shown). EPSC latency at WT synapses was reduced from 1.31 ± 0.05 ms to 1.09 ± 0.04 ms (p = 0.05, Student's t test; data not shown); EPSC latency at Cplx3$^{-/-}$ synapses was unaffected.

Increasing extracellular $[Ca^{2+}]$ ($[Ca^{2+}]_E$) reverses deficits in evoked release at other Cplx$^{-/-}$ synapses (Reim et al., 2001; Xue et al., 2008). At WT and Cplx3$^{-/-}$ RB → AII synapses, 4 mM (Figure 1F) or 8 mM (data not shown) $[Ca^{2+}]_E$ did not increase EPSC amplitude, consistent with saturation of synaptic release machinery at physiological $[Ca^{2+}]_E$ (Jarsky et al., 2010). Elevated $[Ca^{2+}]_E$, however, decreased EPSC latency at WT and Cplx3$^{-/-}$ synapses, with a relative delay persisting at Cplx3$^{-/-}$ synapses (Figure 1G). We conclude that the efficiency with which Ca^{2+} elicits exocytosis is reduced at Cplx3$^{-/-}$ RB → AII synapses. This likely reflects an impaired action of Ca^{2+} on the release machinery, downstream of Ca^{2+} binding to its sensor, rather than altered physical coupling between Ca channels and release sites.

Loss of Cplx3 from RBs Increases Spontaneous, Ca^{2+}-Dependent Exocytosis

Cplxs appear to suppress spontaneous exocytosis and, thereby, preserve vesicles in a release-ready state (Chang et al., 2015; Rizo and Xu, 2015). Therefore, we recorded spontaneous, AMPAR-mediated EPSCs in AIIs in the presence of L-AP4, a mGluR6 agonist that hyperpolarizes presynaptic RBs and reduces spontaneous EPSC frequency; spontaneous EPSCs in this condition are presumed to be quantal, miniature EPSCs (mEPSCs) (Jarsky et al., 2010; Mehta et al., 2013; Singer et al., 2004). These mEPSCs reflect spontaneous release from ~100 AZs in seven to ten separate RBs presynaptic to the recorded AII (Tsukamoto and Omi, 2013).

Spontaneous mEPSC frequency was doubled at Cplx3$^{-/-}$ synapses, although mEPSC amplitude and time course were unchanged (Figures 2A–2C). A recent study of isolated mouse RBs also reported increased spontaneous release, inferred from membrane capacitance recordings and FM4–64 destaining, after antagonizing Cplx3 with a blocking peptide (Vaithianathan et al., 2015). However, the effect of the blocking peptide is ~10-fold higher than what we observed at Cplx3$^{-/-}$ RB → AII synapses: if vesicle capacitance ≈ 25 aF (Zhou et al., 2006), the reported ~200-fF increase in 40 s equates to a release rate of 200 vesicles × s^{-1} versus the 18 vesicles × s^{-1} observed here (Figure 2C). Dissociation of RBs,

then, seems to have a far larger effect on the stability of vesicle pools at AZs than does Cplx3, likely owing to the extensive interactions between presynaptic proteins (e.g., Ca channels) and elements in the extracellular matrix and on postsynaptic cell(s) (Bemben et al., 2015).

At RB → AII synapses, mEPSC frequency depends on $[Ca^{2+}]_E$ (Mehta et al., 2013; Singer et al., 2004). Eliminating $[Ca^{2+}]_E$ (0 mM + 5 mM Egta external) reduced mEPSC frequency at both WT and Cplx3$^{-/-}$ synapses to statistically similar values (Figures 2D and 2E). Thus, elevated spontaneous release from Cplx3$^{-/-}$ RB terminals was Ca^{2+} dependent, and Ca^{2+} influx at resting V_M was sufficient to elevate $[Ca^{2+}]_I$ to evoke spontaneous exocytosis. Consistent with this, the fluorescence of GCaMP3 expressed in RBs varied with $[Ca^{2+}]_E$ (Figure S2A). We conclude that Cplx3 does not affect constitutive, Ca^{2+}-independent exocytosis but rather exerts a clamping effect on spontaneous, Ca^{2+}-mediated vesicle fusion.

Coordinated Multivesicular Release Is Preserved in Cplx3$^{-/-}$ Synapses

Ribbon synapses, including those of RBs, exhibit coordinated multivesicular release (MVR): the near-simultaneous exocytosis of multiple vesicles at the same AZ (Chapochnikov et al., 2014). Though the underlying mechanism is uncertain (Chapochnikov et al., 2014), MVR apparently reflects a high initial release probability (P_R) RRP, because it is eliminated by synaptic depression arising from vesicle depletion (Singer and Diamond, 2006; Singer et al., 2004). Given the apparent reduction in RRP and P_R (i.e., attenuation of phasic EPSCs) at Cplx3$^{-/-}$ synapses and the suggestion that MVR might depend on $[Ca^{2+}]_I$ nanodomains (Graydon et al., 2011; Jarsky et al., 2010), we tested for coordinated MVR from Cplx3$^{-/-}$ RBs.

Depolarization of RBs to the threshold for exocytosis (approximately −51 mV for 300 ms; Figure 3A, top) evoked coordinated MVR (n = 8). For WT synapses, this stimulus generated I_{Ca} = 3.3 ± 0.8 pA and evoked desynchronized EPSCs with QC (QC = ∫EPSC ÷ ∫mEPSC) = 1.3 ± 0.1 but with waveforms identical to those of the mEPSC (Figure 3B). As a control, short pre-pulse depolarizations to −20 mV that depleted the presynaptic RRP reduced subsequent desynchronized EPSC QC to the quantal level (Figure 3B) (Singer et al., 2004).

Surprisingly, we observed coordinated MVR at Cplx3$^{-/-}$ synapses (Figure 3A, bottom) (n = 11). The RB voltage threshold for exocytosis was significantly higher (approximately −44 mV; Figures 1D and 1E), and more Ca^{2+} influx was required to evoke EPSCs (I_{Ca} = 12.2 ± 1.2 pA). But at Cplx3$^{-/-}$ synapses, as at WT synapses, evoked desynchronized EPSCs were multiquantal (QC = 1.3 ± 0.1) and followed the same time course as mEPSCs (Figure 3B). The frequency of desynchronized EPSCs was higher at Cplx3$^{-/-}$ synapses (WT versus Cplx3$^{-/-}$: 73 ± 14 versus 166 ± 18 vesicles • s^{-1}), likely owing to the increased I_{Ca} necessary to evoke transmission. Most interestingly, pre-pulses had no effect on event amplitude (Figure 3B). Coordinated MVR did not persist at Cplx3$^{-/-}$ synapses simply by chance: the probability that two vesicles underwent exocytosis within a brief (100-μs) time window was 0.001, given event frequency ≈ 160 • s^{-1} arising from ~15 AZs in a paired recording (Tsukamoto and Omi, 2013).

Coordinated MVR at Cplx3$^{-/-}$ synapses might involve a vesicle pool separate from the high P_R RRP. Experimental evidence, however, opposes this suggestion: depletion of the RRP eliminates MVR (Singer et al., 2004) (Figures 3A and 3B). Alternatively, coordinated MVR might result from a delayed priming process requiring sustained elevation in $[Ca^{2+}]_I$ on the order of several milliseconds. Consistent with this second explanation, coordinated MVR is observed in asynchronous EPSCs that depend on globally elevated $[Ca^{2+}]_I$ following the closure of Ca channels (Kaeser and Regehr, 2014; Kavalali, 2015; Singer et al., 2004). Furthermore, latency to the first evoked desynchronized event approximately doubled at Cplx3$^{-/-}$ synapses (WT versus Cplx3$^{-/-}$: 3.9 ± 0.1 ms versus 8.6 ± 1.2 ms; data not shown), suggesting increased dependence of transmission on globally elevated $[Ca^{2+}]_I$. Thus, coordinated MVR in the absence of Cplx3 provides functional evidence of an appropriate number of releasable vesicles present at Cplx3$^{-/-}$ RB AZs. Ultrastructural analysis confirmed this prediction (Figure S1M).

Recovery of Phasic Transmission Is Impaired at Cplx3$^{-/-}$ Synapses

Phasic transmission at RB → AII synapses shows strong use-dependent depression arising from RRP depletion (Jarsky et al., 2011; Ke et al., 2014; Oesch and Diamond, 2011). Depression at hippocampal synapses is reduced by loss of Cplx1/2/3 (Xue et al., 2008); therefore, we tested whether depression at Cplx3$^{-/-}$ RB synapses was altered similarly. During 100-Hz stimulus trains, WT synapses depressed rapidly; EPSC amplitudes reached a steady state ~20% of the first within four responses (Figures 4A–4C, black). Cplx3$^{-/-}$ synapses depressed initially at the same rate as WT synapses, but EPSC amplitudes recovered to a steady state ~75% of the first within ten responses (Figures 4A–4C, red). EPSCs at Cplx3$^{-/-}$ synapses were much smaller in amplitude than those at WT synapses, indicating a profound reduction in the functional RRP (Figure 4A, inset).

Recovery rate was determined by integrating the EPSC train (Figure 4D; note a diminished initial integral amplitude, indicating reduced RRP size), dividing the integrals into five 100-ms-duration sections and fitting the final four (beginning 100 ms after train onset) with straight lines (Figure 4E). Recovery rate at WT, but not Cplx3$^{-/-}$, synapses slowed with time.

To quantify the recovery rate of phasic transmission alone, we eliminated contributions of slow modes of exocytosis driven by elevated $[Ca^{2+}]_I$ during the stimulus train by integrating individual EPSCs after subtracting a 1-ms baseline preceding each stimulus (Figure 4F). Integrals were divided into five 100-ms sections, and lines fit to WT, but not Cplx3$^{-/-}$, data were reduced in slope as sections advanced (Figure 4G). Slopes of lines fit to the 100- to 200-ms and the 200- to 300-ms bins differed significantly between WT and Cplx3$^{-/-}$, indicating that the recovery of phasic transmission at RB synapses occurred in several phases, the earlier of which required Cplx3. Imaging $[Ca^{2+}]$ indicator fluorescence in RB terminals during the stimulus train indicated that the observed defect in recovery from depression was not due to differences in $[Ca^{2+}]_I$ dynamics between WT and Cplx3$^{-/-}$ RB terminals (Figure S2B).

Loss of Cplx3 Alters Transmission of Rod Signals through the RB Pathway

We recorded retinal light responses to assess the functional significance of Cplx3 to transmission at RB → AII synapses. In dim light, rod output is propagated to GCs, the retinal output neurons, by the RB pathway as follows: rod → RB → AII → ON cone bipolar cell (CB) → ON GC (Ke et al., 2014). One type of GC, the ONαGC, receives particularly strong input from the RB pathway via type 6 ON CBs coupled electrically to AIIs (Schwartz et al., 2012). We recorded RB pathway-mediated responses from AIIs and ONαGCs in whole mounts of dark-adapted WT and Cplx3$^{-/-}$ retinas (Figure 5); the stimulus, activating rods primarily, was a green spot (320 μm diameter) modulated at 1 Hz around a mean luminance that generated ~10 rhodopsin isomerations per rod per second (R*/rod/s) (20%–100% contrast modulation).

Consistent with increased spontaneous release at Cplx3$^{-/-}$ RB → AII synapses (Figure 2), membrane currents of AIIs (I_{AII}) showed increased synaptic noise (i.e., variance at mean luminance) in Cplx3$^{-/-}$ relative to WT retinas (Figure 5A3). Contrast modulation elicited I_{AII} with similar peak-to-peak amplitude in WT and Cplx3$^{-/-}$ retinas (Figure 5A4), but I_{AII} in Cplx3$^{-/-}$ was slowed in time course. In particular, RB → AII synapses in Cplx3$^{-/-}$ showed reduced ability to cease exocytosis following decrements in luminance (i.e., the "OFF" response was delayed). We quantified this delay by Fourier analysis of the response and measurement of phase at the fundamental (1 Hz) frequency (Figures 5A1 and 5A5). Relative to WT, phase was systematically delayed in Cplx3$^{-/-}$ (Figure 5A5). The slowed shutoff of light-evoked release onto AIIs during the OFF response could be explained by increased asynchronous release at Cplx3$^{-/-}$ RB synapses.

Recording light-evoked changes in AII V_M tested the hypothesis that increased spontaneous and asynchronous transmission at RB → AII synapses would make AIIs in Cplx3$^{-/-}$ retinas more depolarized than those in WT retinas (Figure 5B1). Measurements of V_M at mean luminance were variable (Figure 5B2), and although differences were not significant, there was a trend toward more depolarized AIIs in Cplx3$^{-/-}$ retinas ($p < 0.10$, one-tailed Student's t test). Light-evoked voltage changes, however, were altered significantly in AIIs of Cplx3$^{-/-}$ retinas: responses showed both reduced peak-to-peak amplitudes and F1 phase delays (Figures 5B4 and 5B5); the latter finding is consistent with recordings of membrane current. The reduction in the voltage, but not current, response amplitude suggests a reduced driving force on excitatory synaptic conductances in AIIs at Cplx3$^{-/-}$ synapses; this is consistent with our finding that average V_M in AIIs during the stimulus (measured over four cycles, 100% contrast) was depolarized significantly in the Cplx3$^{-/-}$ retina (Figure 5B1).

We recorded light-evoked currents in ONαGCs(I_{GC}) (Figure 5C) to examine the consequence of altered AII responses. I_{GC} variance was lowered significantly in the Cplx3$^{-/-}$ retina, indicating reduced release from presynaptic ON CBs (Figure 5C3). Furthermore, responses to modulated contrast were attenuated by ~4-fold in amplitude (Figure 5C4), a far larger reduction than the ~1.5-fold difference observed in I_{AII} (Figure 5B4). I_{GC} in Cplx3$^{-/-}$ retinas also showed delayed F1 phase (Figure 5C5). I_{GC} from Cplx3$^{+/+}$ littermate controls resembled that recorded from C57B6 controls (Figures 5C2–5C5). The attenuation in I_{GC} amplitude in Cplx3$^{-/-}$ retinas was preserved across a range of contrasts around the same mean luminance (20, 40% at 10 R*/rod/s; Figure 6A) and at a

higher mean luminance (but still primarily rod activating; 100% contrast, 100 R*/rod/s; Figure 6B).

The strong attenuation of I_{GC} amplitude in Cplx3$^{-/-}$ retinas did not reflect an unexpected effect of Cplx3 deletion on the presynaptic ON CBs, which are thought not to express Cplx3 (Reim et al., 2009): indeed, I_{GC} evoked by contrast in bright UV light (mean: 10,000 R* per cone per second [R*/cone/s]) that activated cones and ON CBs independent from the RB pathway were relatively normal in Cplx3$^{-/-}$ retinas (Figure 6C). Dimming the UV stimulus 1,000-fold (10 R*/cone/s) into a range encoded by RBs yielded more sluggish I_{GC} in Cplx3$^{-/-}$ retinas, similar to that evoked by the dim green stimuli used earlier (Figure 6C); here, we also observed a shift in F1 phase (Figure 6D). Thus, ON CBs in Cplx3$^{-/-}$ retinas apparently function normally.

The reduced and delayed RB-pathway-mediated responses recorded in ONαGCs likely result from the depolarization of ON CB terminals as a consequence of depolarized V_M in electrically coupled AIIs; sustained depolarization of ON CB terminals would induce use-dependent synaptic depression, likely resulting from RRP depletion (Grimes et al., 2014). We tested this postulate by hyperpolarizing the AII-ON CB network in Cplx3$^{-/-}$ and WT retinas. Because resting V_M of AIIs is influenced strongly by a M-type K conductance (Cembrowski et al., 2012), we used the M-current (Kv7 channel) activator flupirtine (10 μM) to hyperpolarize AIIs (Choi et al., 2014): in slices of Cplx3$^{-/-}$ retina, flupirtine reduced AII V_M from −42.5 ± 1.3 to −51.7 ± 0.7 mV (n = 9; $p < 0.0001$ by Student's t test; data not shown). This hyperpolarization would be propagated to the terminals of ON CBs (Grimes et al., 2014), and we assessed its effect on I_{GC} evoked by input from the RB pathway.

During steady illumination (mean = 10 R*/rod/s), flupirtine increased holding current in recordings of four out of six ONαGCs in the Cplx3$^{-/-}$ retina, consistent with its increasing tonic release from presynaptic ON CBs by hyperpolarizing them enough to permit recovery from synaptic depression (Figures 6E and 6F). Furthermore, flupirtine increased amplitudes of responses to modulated contrast (100%; mean = 10 R*/rod/s) in six out of six cells (Figures 6E and 6F). In ONαGCs in WT retinas, flupirtine caused the opposite effects: holding current was reduced, and response amplitude was diminished slightly. Presumably, by hyperpolarizing coupled AIIs, flupirtine hyperpolarized ON CB terminals in the WT retina sufficiently to attenuate transmission at ON CB → ONαGC synapses. Across all ONαGCs, the effect of flupirtine on holding current was correlated with the effect on response amplitude: when holding current increased (i.e., became more negative), response amplitude increased, and vice versa (Figure 6F). Thus, flupirtine apparently partially reversed use-dependent depression of ON CB → ONαGC synapses by hyperpolarizing the AII-ON CB network.

Asynchronous Release at Cplx3$^{-/-}$ Synapses Is Enhanced

Cplx3$^{-/-}$ RB → AII synapses showed delayed "OFF" responses to contrast stimuli, suggesting that Ca^{2+}-dependent exocytosis persisted after RBs were hyperpolarized at light offset. Therefore, we examined asynchronous transmission at RB → AII synapses in more detail by paired recording in retinal slices. RB V_M was modulated with a voltage waveform

(1 Hz square wave; −60 ± 15 mV) designed to resemble the presumed RB response to the contrast stimulus.

At WT synapses, depolarization evoked EPSCs with both phasic and sustained components; EPSCs at Cplx3$^{-/-}$ synapses exhibited weak phasic but intact sustained components (Figures 7A and 7B). During hyperpolarization phases, release did not cease completely at either WT or Cplx3$^{-/-}$ synapses, but asynchronous events occurred at a higher frequency at Cplx3$^{-/-}$ synapses (Figure 7C). After the stimulus ended, release frequency decayed to baseline more slowly at Cplx$^{-/-}$ synapses (Figures 7A–7C). Thus, slowing of the light-evoked I_{AII} waveform in Cplx3$^{-/-}$ retinas (Figures 5 and 6) seemed to depend on excess asynchronous release from RBs. Additionally, reduced phasic release at Cplx3$^{-/-}$ synapses probably explains the delayed light responses of AIIs in Cplx3$^{-/-}$ retinas under low-contrast conditions (Figure 7A).

Additional investigation revealed that the clamping function of Cplx3 on asynchronous release is not essential when $[Ca^{2+}]_I$ is effectively buffered. We did not observe enhanced asynchronous release at Cplx3$^{-/-}$ synapses following brief (5–100 ms) presynaptic depolarizations in physiological (1.15 mM) $[Ca^{2+}]_E$ (Figures 7D and 7E); this condition is not expected to raise $[Ca^{2+}]_I$ significantly (Mehta et al., 2014). Increasing $[Ca^{2+}]_I$, either by elevating $[Ca^{2+}]_E$ and reducing $[Bapta]_I$ (Figure 7F) or by lengthening RB depolarization to 1,000 ms (1.15 mM $[Ca^{2+}]_E$; Figure 7G), however, led to a relative enhancement in asynchronous release at Cplx3$^{-/-}$ synapses. Notably, we observed a delayed-release component in EPSCs evoked by 1,000 ms depolarizations. Although delayed release appeared mildly slowed in onset and slightly larger at Cplx3$^{-/-}$ synapses (WT versus Cplx3$^{-/-}$: 23.1 ± 5.4 versus 44.9 ± 8.1 pC; $p = 0.036$), given the difficulty of separating asynchronous from delayed components of release, the increased delayed charge transfer likely reflected enhanced asynchronous release. This interpretation is consistent with the description of Cplx as a clamp on asynchronous release (Chang et al., 2015).

DISCUSSION

Loss of Cplx3 at RB → AII synapses diminished phasic release while enhancing Ca^{2+}-dependent spontaneous and asynchronous release (Figures 1, 2, and 4). Impaired phasic release was manifested both in a reduced functional RRP and in an increased EPSC latency. The diminished functional RRP likely resulted from the absence of a facilitatory effect of Cplx3 on Ca^{2+}-dependent exocytosis (Figure 4) rather than from physical vesicle depletion (Figure S1). Enhanced asynchronous release, reflecting the removal of a Cplx3-mediated brake on unregulated Ca^{2+}-dependent exocytosis, slowed light-evoked signaling in the AII network, thereby attenuating propagation of rod-derived signals to GCs (Figures 5, 6, and 7). Our study supports the growing consensus that Cplxs (Cplx3 in RBs and Cplx1 and Cplx2 at conventional synapses) act to stabilize fully primed vesicles in a release-ready state and to suppress unregulated Ca^{2+}-dependent spontaneous and asynchronous release of immature vesicles at early stages of the priming process (Chang et al., 2015; Hobson et al., 2011; Martin et al., 2011; Maximov et al., 2009; Trimbuch and Rosenmund, 2016; Xue et al., 2010; Yang et al., 2010).

Cplx3 and the Efficiency of Ca^{2+} Exocytosis Coupling

$[Ca^{2+}]_I$ in nanodomains generated by the opening of single Ca channels can control exocytosis of primed vesicles from RB AZs on millisecond timescales (Jarsky et al., 2010). Absent diffusion barriers to confine Ca^{2+} (Bartoletti et al., 2011; Graydon et al., 2011), one open Ca channel generates a rapidly dissipating, moderate $[Ca^{2+}]_I$ change <10 μM at an ~10-nm distance (Jarsky et al., 2010; Neher, 1998); nanodomain control, then, indicates that the efficiency with which Ca^{2+} evokes exocytosis is high.

Cplxs lower the free-energy barrier to membrane fusion to increase the efficiency of Ca^{2+}-dependent exocytosis (Cai et al., 2008; Krishnakumar et al., 2011; Kümmel et al., 2011; Li et al., 2011); several observations indicate that Cplx3 acts in this manner at RB AZs. $Cplx3^{-/-}$ synapses exhibited decreased phasic release, indicating a reduced RRP (Figures 1 and 4). The slowed early recovery phase of phasic transmission from use-dependent depression in the absence of Cplx3 (Figure 4) is also consistent with a smaller number of available release sites resulting from the reduced RRP size.

The small RRP at $Cplx3^{-/-}$ synapses reflects reduced efficiency in Ca^{2+}-dependent exocytosis of primed vesicles. Increasing Ca^{2+} influx into the RB terminal and the spatial spread of $[Ca^{2+}]_I$ by raising $[Ca^{2+}]_E$ and reducing $[Bapta]_I$ did not alter the $Cplx3^{-/-}$ phenotype (Figures 1F and 1G). Further, $Cplx3^{-/-}$ synapses exhibited an elevated RB voltage (and I_{Ca}) threshold for exocytosis (Figures 1E and 4A). Thus, the facilitatory effect of Cplx3 either acts independently of Ca^{2+} or follows Ca^{2+} binding to the primed release machinery. As Cplxs interact with the SNARE complex and cooperate with the Ca^{2+} sensor synaptotagmin (Xue et al., 2010), we favor the latter hypothesis.

$Cplx3^{-/-}$ synapses showed inhibition of phasic transmission coupled with enhancement of Ca^{2+}-dependent spontaneous (Figures 2 and 6) and asynchronous (Figure 7) release. The role of Cplx3 in enhancing the efficiency of exocytosis, therefore, is linked closely to its role in inhibiting unregulated (premature) release of vesicles before they are fully primed. In the absence of Cplx3, vesicles undergoing the priming process are lost to unregulated (spontaneous and/or asynchronous) exocytosis driven by global $[Ca^{2+}]_I$. Notably, the "unclamping" of both Ca^{2+}-dependent spontaneous and asynchronous release at $Cplx3^{-/-}$ synapses adds to mounting evidence that these two release modes draw on a common vesicle pool that may be molecularly distinct from the RRP (Kaeser and Regehr, 2014; Kavalali, 2015; Schneggenburger and Rosenmund, 2015).

Our EM analysis indicates that the diminished RRP, assessed functionally, did not result from a physical depletion of vesicles from ribbon AZs (Figures S1H–S1M), although we cannot exclude the possibility of subtle changes in positions of vesicles relative to Ca channels (Figure S1N). As well, the observed coordinated MVR, which draws on the RRP (Singer et al., 2004), at $Cplx3^{-/-}$ RB → AII synapses (Figure 3) provides strong evidence against a physical depletion of vesicles.

Mechanisms of Coordinated MVR

Coordinated MVR is observed at photoreceptor, bipolar cell, and hair cell ribbon synapses. Proposed mechanisms for coordination include: (1) release site coordination, possibly by

$[Ca^{2+}]_I$ nanodomains; (2) compound fusion of vesicles prior to or during exocytosis; and (3) the possibility that MVR is not MVR at all but rather reflects variable emptying of a single vesicle through a flickering fusion pore (Chapochnikov et al., 2014).

MVR at RB → AII synapses presumably results from release site coordination because it obeys binomial statistics (Jarsky et al., 2010; Singer et al., 2004). Furthermore, it is thought to result from a high initial P_R because it is $[Ca^{2+}]$ dependent and eliminated by synaptic depression arising from vesicle depletion; this latter observation indicates that MVR and phasic release draw on the same vesicle pool (Jarsky et al., 2010; Singer et al., 2004). Consequently, it was surprising to observe MVR at Cplx3$^{-/-}$ RB → AII synapses, which exhibit a diminished RRP and increased reliance on global $[Ca^{2+}]_I$ for exocytosis. Apparently, then, MVR is not simply a reflection of initial P_R. Instead, MVR appears to arise from some delayed, Ca^{2+}-dependent process acting on vesicles in the RRP.

Insight into Signal Processing by the RB Pathway

Responses of ONαGCs to input from the RB pathway were altered significantly in Cplx3$^{-/-}$ retinas (Figures 5 and 6). ONαGC responses to cone stimulation (cone → ON CB → ONαGC) were normal in Cplx3$^{-/-}$ retinas, demonstrating that ON CB → ONαGC synapses were not affected (Figure 6C). The deficit in ONαGC responses reflected a slowing of transmission at RB → AII synapses (Figures 5 and 6) arising largely from asynchronous release potentiated by the absence of Cplx3 (Figure 7A). Despite reduced phasic transmission at Cplx3$^{-/-}$ RB synapses, amplitudes of light-evoked currents in AIIs were largely unchanged in Cplx3$^{-/-}$ retinas (Figures 5 and 6); this is consistent with normal scotopic electroretinography (ERG) b-waves observed in Cplx3$^{-/-}$ animals (Reim et al., 2009).

Light-evoked currents in the ONαGCs of WT retinas were rectified, with large, transient components elicited by light onset and an almost complete cessation of charge flux at light offset, whereas currents in Cplx3$^{-/-}$ retinas were less rectified and changed slowly and approximately equivalently by positive and negative contrast (Figure 5). AII V_M modulates transmission at ON CB → ONαGC synapses by moving ON CB V_M relative to the conductance-voltage (G-V) relationship of presynaptic Ca channels (Grimes et al., 2014). Experiments with flupirtine (Figures 6E and 6F), which hyperpolarizes AIIs, generally support the hypothesis that the depolarization of AIIs moves ON CB V_M into a depolarized range in which the G-V relationship of Ca channels is linear; hyperpolarization of the AII moves ON CB V_M into a hyperpolarized range in which the G-V relationship is non-linear (i.e., the foot of the sigmoidal G-V relationship). Thus, the timing of transmission at the RB → AII synapse controls AII V_M, which then serves as the primary determinant of the timing of signaling at ON CB → ONαGC synapses. Enhanced asynchronous release in the Cplx3$^{-/-}$ retina compromised visual signal processing, providing a clear example of how the suppression of desynchronized release modes is critical for precise coding of neural signals at CNS synapses.

EXPERIMENTAL PROCEDURES

Recordings from Retinal Whole Mounts

Retinas from dark-adapted Cplx3$^{-/-}$, littermate Cplx3$^{+/+}$, or C57B6 mice (1–6 months old) (Reim et al., 2009) were isolated under IR illumination, mounted on filter paper, and maintained in a chamber of a two-photon microscope. Whole-cell recordings were made from GCs and amacrine cells (ACs) as described previously (Borghuis et al., 2013; Ke et al., 2014). The Animal Care and Use Committee of Yale University approved all procedures involving animal use. Retinas were superfused with Ames' medium at ~31–32°C, with flupirtine (10 μM; Tocris) added in some experiments.

The pipette solution was Cs based (most voltage-clamp recordings) or K based (current-clamp recordings), as described previously (Park et al., 2015). In some cases, we made both voltage- and current-clamp recordings from the same AII (K-based internal); in these cases, the voltage-clamp recordings contributed to measures of response amplitude and phase but not to baseline noise (see Figures 5A2–5A5 and 5B2–5B5). Lucifer Yellow added to the pipette solution allowed cell morphology to be visualized by two-photon laser-scanning microscopy (2PLSM) following recording (Borghuis et al., 2013). Input and access resistances (the latter compensated by 50%) in MΩ were: 62 ± 8 and 28 ± 3, respectively, for ONαGCs; and 198 ± 15 and 69 ± 6, respectively, for AIIs. Voltages were corrected for a −9-mV junction potential.

In most experiments, a light stimulus (0.32-mm-diameter spot) was generated with a green LED (530 nm peak; Ke et al., 2014). In other experiments, the stimulus (0.4-mm-diameter spot) was generated with a modified video projector (395-nm peak; Borghuis et al., 2013); in this case, background was set to mean luminance. The stimulus was focused onto the photoreceptors through the microscope condenser. Neutral density filters were placed in the light path to adjust the mean luminance. For experiments with the green LED stimulus, GC recordings were made in the ventral retina, where the cones express primarily a UV-sensitive opsin. AII recordings were made over a larger region of the retina, depending on where the inner nuclear layer could be clearly visualized with infrared light. Photoisomerization rates were calculated based on a collecting area of 0.85 μm^2 for rods and 1 μm^2 for cones (Wang et al., 2011).

Retinal Slice Recordings

Retinal slices (200 μm thick) were prepared from light-adapted Cplx3$^{-/-}$ and littermate Cplx3$^{+/+}$ mice (1–6 months old) (Reim et al., 2009), and recordings from RBs and AIIs were made as described previously (Jarsky et al., 2011). The Animal Care and Use Committee of the University of Maryland approved all procedures involving animal use, and all animal procedures performed in Germany were conducted with permission from the Landesamt für Verbraucherschutz und Lebensmittelsicherheit Niedersachsen, Oldenburg, Germany. Slices were superfused with a warmed (~34°C), carbogen-bubbled artificial cerebrospinal fluid, to which blockers of $GABA_AR$-, $GABA_CR$-, GlyR-, voltage-gated Na channel-, mGluR6-regulated channel-, and Ca^{2+}-activated Cl channel-mediated currents were added (Jarsky et al., 2011). Generally, RB holding potential was −60 mV, AII holding potential was −80 mV,

and both were corrected for junction potentials of −10 mV. Access resistances were <25 MΩ for RBs and <20 MΩ for AIIs and were compensated by 50%–90%. Access resistances for AII recordings made in retinal slices were lower than those made in whole-mount preparations, owing to the relative ease of maintaining an unobstructed recording pipette in the slice.

Statistical Methods

All data are presented as mean ± SEM with n values. Differences between experimental observations were tested for significance, taken as $p < 0.05$, using Student's t tests, ANOVA, and the Wilcoxon signed-rank test as noted.

Supplementary Material

Refer to Web version on PubMed Central for supplementary material.

Acknowledgments

This study was supported by the Max Planck Society (N.B.), the German Research Foundation (SFB889/B1 to N.B. and J.-S.R.), NIH grants EY017836 to J.H.S., EY021372 to J.H.S. and J.B.D., and an unrestricted grant from Research to Prevent Blindness to the Department of Ophthalmology at Yale University. We thank M. Tong and A. Günther for technical assistance.

REFERENCES

Bartoletti TM, Jackman SL, Babai N, Mercer AJ, Kramer RH, Thoreson WB. Release from the cone ribbon synapse under bright light conditions can be controlled by the opening of only a few Ca($^{2+}$) channels. J. Neurophysiol. 2011; 106:2922–2935. [PubMed: 21880934]

Bemben MA, Shipman SL, Nicoll RA, Roche KW. The cellular and molecular landscape of neuroligins. Trends Neurosci. 2015; 38:496–505. [PubMed: 26209464]

Borghuis BG, Marvin JS, Looger LL, Demb JB. Two-photon imaging of nonlinear glutamate release dynamics at bipolar cell synapses in the mouse retina. J. Neurosci. 2013; 33:10972–10985. [PubMed: 23825403]

Cai H, Reim K, Varoqueaux F, Tapechum S, Hill K, Sørensen JB, Brose N, Chow RH. Complexin II plays a positive role in Ca2+-triggered exocytosis by facilitating vesicle priming. Proc. Natl. Acad. Sci. USA. 2008; 105:19538–19543. [PubMed: 19033464]

Cembrowski MS, Logan SM, Tian M, Jia L, Li W, Kath WL, Riecke H, Singer JH. The mechanisms of repetitive spike generation in an axonless retinal interneuron. Cell Rep. 2012; 1:155–166. [PubMed: 22832164]

Chang S, Reim K, Pedersen M, Neher E, Brose N, Taschenberger H. Complexin stabilizes newly primed synaptic vesicles and prevents their premature fusion at the mouse calyx of held synapse. J. Neurosci. 2015; 35:8272–8290. [PubMed: 26019341]

Chapochnikov NM, Takago H, Huang CH, Pangršič T, Khimich D, Neef J, Auge E, Göttfert F, Hell SW, Wichmann C, et al. Uniquantal release through a dynamic fusion pore is a candidate mechanism of hair cell exocytosis. Neuron. 2014; 83:1389–1403. [PubMed: 25199706]

Choi H, Zhang L, Cembrowski MS, Sabottke CF, Markowitz AL, Butts DA, Kath WL, Singer JH, Riecke H. Intrinsic bursting of AII amacrine cells underlies oscillations in the rd1 mouse retina. J. Neurophysiol. 2014; 112:1491–1504. [PubMed: 25008417]

Demb JB, Singer JH. Functional circuitry of the retina. Annu. Rev. Vis. Sci. 2015; 1:263–289.

Graydon CW, Cho S, Li GL, Kachar B, von Gersdorff H. Sharp Ca^{2+} nanodomains beneath the ribbon promote highly synchronous multivesicular release at hair cell synapses. J. Neurosci. 2011; 31:16637–16650. [PubMed: 22090491]

Grimes WN, Schwartz GW, Rieke F. The synaptic and circuit mechanisms underlying a change in spatial encoding in the retina. Neuron. 2014; 82:460–473. [PubMed: 24742466]

Hobson RJ, Liu Q, Watanabe S, Jorgensen EM. Complexin maintains vesicles in the primed state in C. elegans. Curr. Biol. 2011; 21:106–113. [PubMed: 21215631]

Jarsky T, Tian M, Singer JH. Nanodomain control of exocytosis is responsible for the signaling capability of a retinal ribbon synapse. J. Neurosci. 2010; 30:11885–11895. [PubMed: 20826653]

Jarsky T, Cembrowski M, Logan SM, Kath WL, Riecke H, Demb JB, Singer JH. A synaptic mechanism for retinal adaptation to luminance and contrast. J. Neurosci. 2011; 31:11003–11015. [PubMed: 21795549]

Kaeser PS, Regehr WG. Molecular mechanisms for synchronous, asynchronous, and spontaneous neurotransmitter release. Annu. Rev. Physiol. 2014; 76:333–363. [PubMed: 24274737]

Kavalali ET. The mechanisms and functions of spontaneous neurotransmitter release. Nat. Rev. Neurosci. 2015; 16:5–16. [PubMed: 25524119]

Ke J-B, Wang YV, Borghuis BG, Cembrowski MS, Riecke H, Kath WL, Demb JB, Singer JH. Adaptation to background light enables contrast coding at rod bipolar cell synapses. Neuron. 2014; 81:388–401. [PubMed: 24373883]

Krishnakumar SS, Radoff DT, Küummel D, Giraudo CG, Li F, Khandan L, Baguley SW, Coleman J, Reinisch KM, Pincet F, Rothman JE. A conformational switch in complexin is required for synaptotagmin to trigger synaptic fusion. Nat. Struct. Mol. Biol. 2011; 18:934–940. [PubMed: 21785412]

Küummel D, Krishnakumar SS, Radoff DT, Li F, Giraudo CG, Pincet F, Rothman JE, Reinisch KM. Complexin cross-links prefusion SNAREs into a zigzag array. Nat. Struct. Mol. Biol. 2011; 18:927–933. [PubMed: 21785414]

Landgraf I, Müuhlhans J, Dedek K, Reim K, Brandstätter JH, Ammermüuller J. The absence of Complexin 3 and Complexin 4 differentially impacts the ON and OFF pathways in mouse retina. Eur. J. Neurosci. 2012; 36:2470–2481. [PubMed: 22694764]

Li F, Pincet F, Perez E, Giraudo CG, Tareste D, Rothman JE. Complexin activates and clamps SNAREpins by a common mechanism involving an intermediate energetic state. Nat. Struct. Mol. Biol. 2011; 18:941–946. [PubMed: 21785413]

Martin JA, Hu Z, Fenz KM, Fernandez J, Dittman JS. Complexin has opposite effects on two modes of synaptic vesicle fusion. Curr. Biol. 2011; 21:97–105. [PubMed: 21215634]

Matthews G, Fuchs P. The diverse roles of ribbon synapses in sensory neurotransmission. Nat. Rev. Neurosci. 2010; 11:812–822. [PubMed: 21045860]

Maximov A, Tang J, Yang X, Pang ZP, Süudhof TC. Complexin controls the force transfer from SNARE complexes to membranes in fusion. Science. 2009; 323:516–521. [PubMed: 19164751]

Mehta B, Snellman J, Chen S, Li W, Zenisek D. Synaptic ribbons influence the size and frequency of miniature-like evoked postsynaptic currents. Neuron. 2013; 77:516–527. [PubMed: 23395377]

Mehta B, Ke JB, Zhang L, Baden AD, Markowitz AL, Nayak S, Briggman KL, Zenisek D, Singer JH. Global Ca^{2+} signaling drives ribbon-independent synaptic transmission at rod bipolar cell synapses. J. Neurosci. 2014; 34:6233–6244. [PubMed: 24790194]

Neher E. Vesicle pools and Ca2+ microdomains: new tools for understanding their roles in neurotransmitter release. Neuron. 1998; 20:389–399. [PubMed: 9539117]

Oesch NW, Diamond JS. Ribbon synapses compute temporal contrast and encode luminance in retinal rod bipolar cells. Nat. Neurosci. 2011; 14:1555–1561. [PubMed: 22019730]

Park SJ, Borghuis BG, Rahmani P, Zeng Q, Kim IJ, Demb JB. Function and Circuitry of VIP+ Interneurons in the Mouse Retina. J. Neurosci. 2015; 35:10685–10700. [PubMed: 26224854]

Reim K, Mansour M, Varoqueaux F, McMahon HT, Süudhof TC, Brose N, Rosenmund C. Complexins regulate a late step in Ca2+-dependent neurotransmitter release. Cell. 2001; 104:71–81. [PubMed: 11163241]

Reim K, Regus-Leidig H, Ammermüuller J, El-Kordi A, Radyushkin K, Ehrenreich H, Brandstätter JH, Brose N. Aberrant function and structure of retinal ribbon synapses in the absence of complexin 3 and complexin 4. J. Cell Sci. 2009; 122:1352–1361. [PubMed: 19386896]

Rizo J, Xu J. The synaptic vesicle release machinery. Annu. Rev. Biophys. 2015; 44:339–367. [PubMed: 26098518]

Schneggenburger R, Rosenmund C. Molecular mechanisms governing Ca($^{2+}$) regulation of evoked and spontaneous release. Nat. Neurosci. 2015; 18:935–941. [PubMed: 26108721]

Schwartz GW, Okawa H, Dunn FA, Morgan JL, Kerschensteiner D, Wong RO, Rieke F. The spatial structure of a nonlinear receptive field. Nat. Neurosci. 2012; 15:1572–1580. [PubMed: 23001060]

Singer JH, Diamond JS. Sustained Ca2+ entry elicits transient postsynaptic currents at a retinal ribbon synapse. J. Neurosci. 2003; 23:10923–10933. [PubMed: 14645488]

Singer JH, Diamond JS. Vesicle depletion and synaptic depression at a mammalian ribbon synapse. J. Neurophysiol. 2006; 95:3191–3198. [PubMed: 16452253]

Singer JH, Lassová L, Vardi N, Diamond JS. Coordinated multivesicular release at a mammalian ribbon synapse. Nat. Neurosci. 2004; 7:826–833. [PubMed: 15235608]

Trimbuch T, Rosenmund C. Should I stop or should I go? The role of complexin in neurotransmitter release. Nat. Rev. Neurosci. 2016; 17:118–125. [PubMed: 26806630]

Tsukamoto Y, Omi N. Functional allocation of synaptic contacts in microcircuits from rods via rod bipolar to AII amacrine cells in the mouse retina. J. Comp. Neurol. 2013; 521:3541–3555. [PubMed: 23749582]

Vaithianathan T, Henry D, Akmentin W, Matthews G. Functional roles of complexin in neurotransmitter release at ribbon synapses of mouse retinal bipolar neurons. J. Neurosci. 2015; 35:4065–4070. [PubMed: 25740533]

Wang YV, Weick M, Demb JB. Spectral and temporal sensitivity of cone-mediated responses in mouse retinal ganglion cells. J. Neurosci. 2011; 31:7670–7681. [PubMed: 21613480]

Xue M, Stradomska A, Chen H, Brose N, Zhang W, Rosenmund C, Reim K. Complexins facilitate neurotransmitter release at excitatory and inhibitory synapses in mammalian central nervous system. Proc. Natl. Acad. Sci. USA. 2008; 105:7875–7880. [PubMed: 18505837]

Xue M, Craig TK, Xu J, Chao HT, Rizo J, Rosenmund C. Binding of the complexin N terminus to the SNARE complex potentiates synaptic- vesicle fusogenicity. Nat. Struct. Mol. Biol. 2010; 17:568–575. [PubMed: 20400951]

Yang X, Kaeser-Woo YJ, Pang ZP, Xu W, Süudhof TC. Complexin clamps asynchronous release by blocking a secondary Ca(2+) sensor via its accessory α helix. Neuron. 2010; 68:907–920. [PubMed: 21145004]

Zhou ZY, Wan QF, Thakur P, Heidelberger R. Capacitance measurements in the mouse rod bipolar cell identify a pool of releasable synaptic vesicles. J. Neurophysiol. 2006; 96:2539–2548. [PubMed: 16914610]

In Brief

Mortensen et al. link complexin-3-dependent synaptic dynamics at rod bipolar cell ribbon synapses to downstream retinal circuit function during rod-mediated vision. In the absence of complexin 3, enhanced asynchronous release from rod bipolar cells depolarizes the postsynaptic network and hinders transmission at synapses onto retinal ganglion cells.

Highlights

- Cplx3 boosts fast phasic transmitter release while suppressing asynchronous release
- Transmission at rod bipolar cell ribbon synapses is sluggish in absence of Cplx3
- Sustained depolarization of postsynaptic interneurons degrades light-evoked signaling

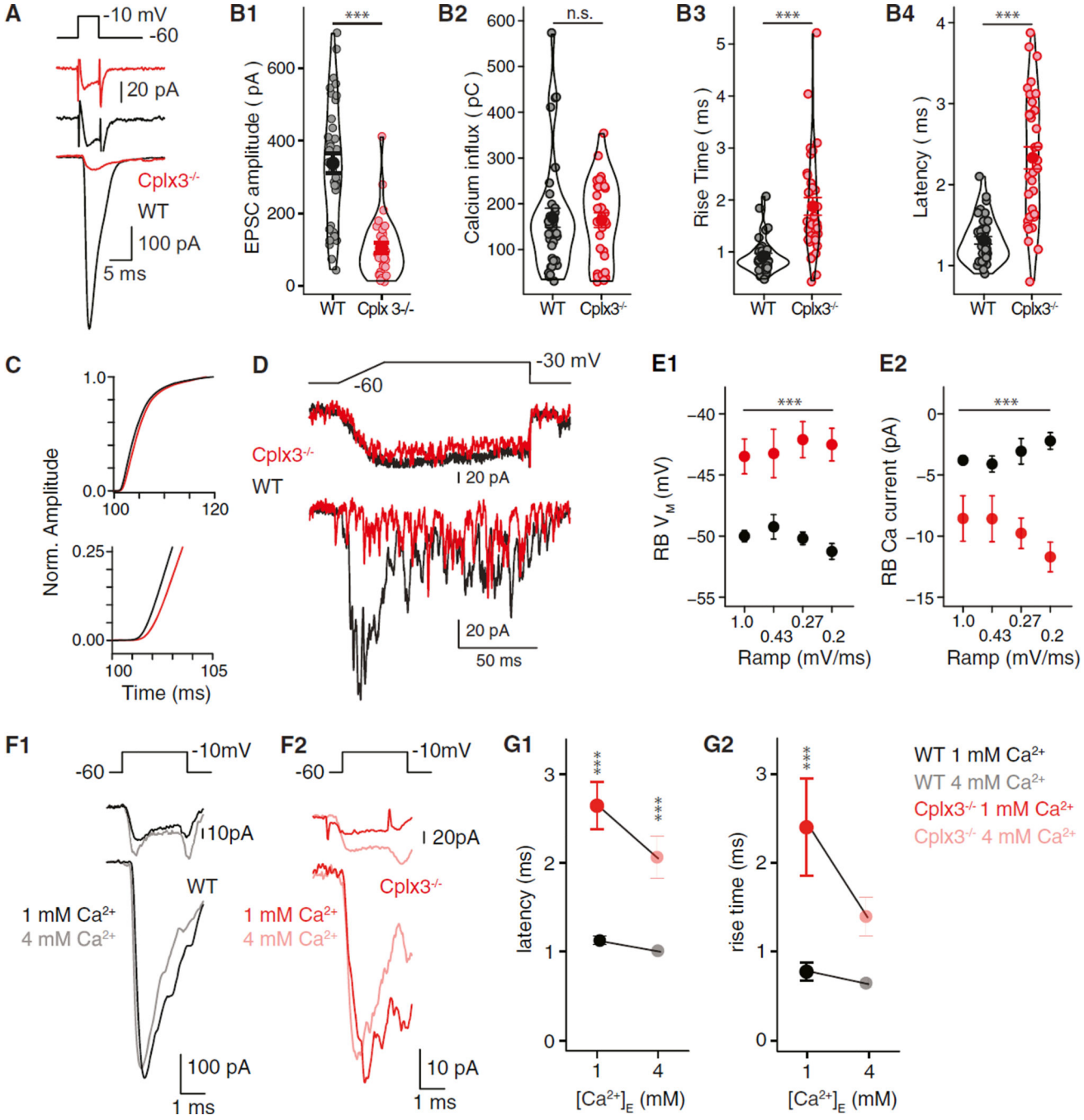

Figure 1. Reduced Phasic Release from Cplx3$^{-/-}$ RBs

(A) Depolarization of RBs (top) elicits RB I_{Ca} (middle) and evokes EPSCs in AIIs (bottom) in WT (black) and Cplx3$^{-/-}$ (red) retina.

(B1–B4) From left: EPSC amplitudes in Cplx3$^{-/-}$ reduced significantly (WT versus Cplx3$^{-/-}$: 338 ± 28 versus 104 ± 14 pA; n = 36 versus 30; $p < 0.0001$), but RB Ca^{2+} influx (integrated I_{Ca}) was unaffected. EPSC rise times and latencies increased in Cplx3$^{-/-}$. The width of outlines around data points represents distribution density.

(C) Integrated EPSCs, normalized (Norm.) to value 20 ms after stimulus onset, illustrate a slowed-release process in Cplx3$^{-/-}$.

(D) RB voltage ramps evoke transient and then desynchronized EPSCs in WT. Transient component is almost abolished in Cplx3$^{-/-}$, but desynchronized events persist.

(E1 and E2) Higher RB V_M threshold for exocytosis in Cplx3$^{-/-}$; first release event is observed at larger RB I_{Ca}.

(F1 and F2) Increasing $[Ca^{2+}]_E$ while reducing $[Bapta]_I$ does not increase EPSC amplitude at either WT or Cplx3$^{-/-}$ synapses; larger RB I_{Ca} in elevated $[Ca^{2+}]_E$.

(G1 and G2) Elevated $[Ca^{2+}]_E$ decreased EPSC latency (left) and rise time (right) in Cplx3$^{-/-}$ but not WT; a relative delay persists in Cplx3$^{-/-}$ (WT versus Cplx3$^{-/-}$: 0.98 versus 2.1 ms; n = 7 versus 6; p = 0.016).

Error bars indicate SEM. We used Student's t test for means in (B), two-way ANOVA for means in (E), and two-way ANOVA with Tukey's honestly significant difference (HSD) post hoc test for (G). **p ≤ 0.01; ***p ≤ 0.001; n.s., not significant.

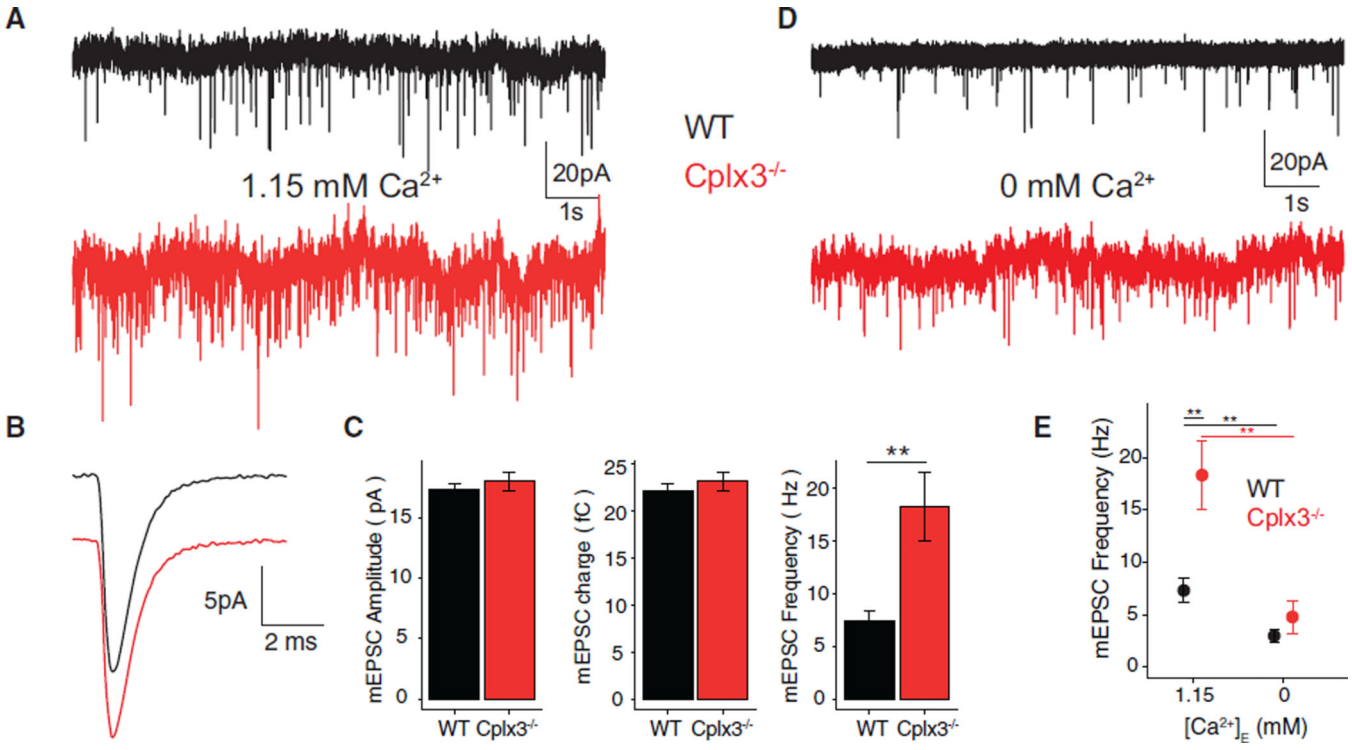

Figure 2. Increased Spontaneous Activity in AIIs at Cplx3$^{-/-}$ Synapses

(A) Recordings from AIIs in WT (black) and Cplx3$^{-/-}$ (red) retinas show increased mEPSC frequency in Cplx3$^{-/-}$.

(B) Average mEPSC waveforms similar in WT and Cplx3$^{-/-}$.

(C) Similar mEPSC amplitude (left), charge (center) in WT and Cplx3$^{-/-}$, and higher mEPSC frequency (right) in Cplx3$^{-/-}$ (WT versus Cplx3$^{-/-}$ frequency: 7.4 ± 1.0 versus 18 vesicles • s^{-1}; n = 26 versus 22; 1.15 mM $[Ca^{2+}]_E$).

(D and E) mEPSC frequencies in WT and Cplx3$^{-/-}$ reduced to similar levels by 0 mM $[Ca^{2+}]_E$ (WT versus Cplx3$^{-/-}$: 2.9 ± 0.7 versus 4.8 ± 1.6 vesicles • s^{-1}; n = 7 each; $p > 0.05$). Error bars indicate SEM. We used Student's t test for WT and Cplx3$^{-/-}$ data at 1.15 mM $[Ca^{2+}]_E$ and two-way ANOVA for frequencies at 1.15 and 0 mM $[Ca^{2+}]_E$. **$p \leq 0.01$.

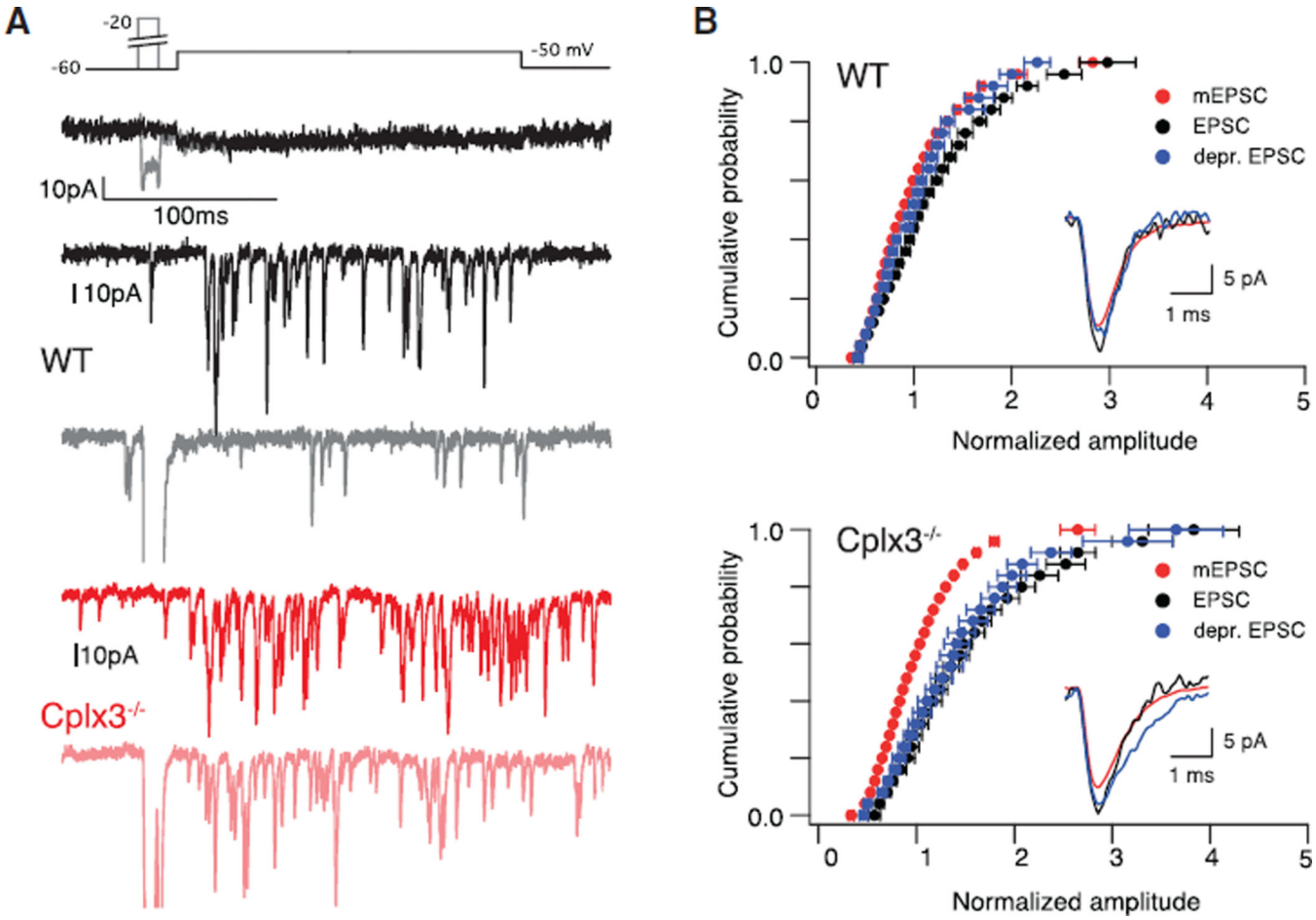

Figure 3. Coordinated MVR from Cplx3$^{-/-}$ RBs

(A) Voltage steps to −50 mV elicit small RB I_{Ca} (top) and evoke desynchronized EPSCs. Prepulse to −20 mV reduces EPSC frequency and amplitude in WT (gray versus black) but not Cplx3$^{-/-}$ (light versus dark red). Stronger presynaptic depolarization used for Cplx3$^{-/-}$ because of elevated RB voltage threshold for exocytosis; see Figure 2D.

(B) Cumulative probability distributions of EPSC amplitudes (red indicates mEPSCs; black indicates control evoked EPSCs; blue indicates evoked EPSCs after pre-pulse) illustrate MVR (n = 8 WT; n = 11 Cplx3$^{-/-}$). Evoked EPSCs and mEPSCs exhibited identical time courses (inset; rise time evoked EPSC versus mEPSC: 0.32 ± 0.01 versus 0.32 ± 0.01 ms for WT and 0.36 ± 0.01 versus 0.34 ± 0.02 ms for Cplx3$^{-/-}$). Evoked EPSC amplitude reduced to quantal level by pre-pulse in WT but not Cplx3$^{-/-}$ (WT: p = 0.008; Cplx3$^{-/-}$: p = 0.8; dependent Wilcoxon signed-rank test). Error bars indicate mean ± SEM.

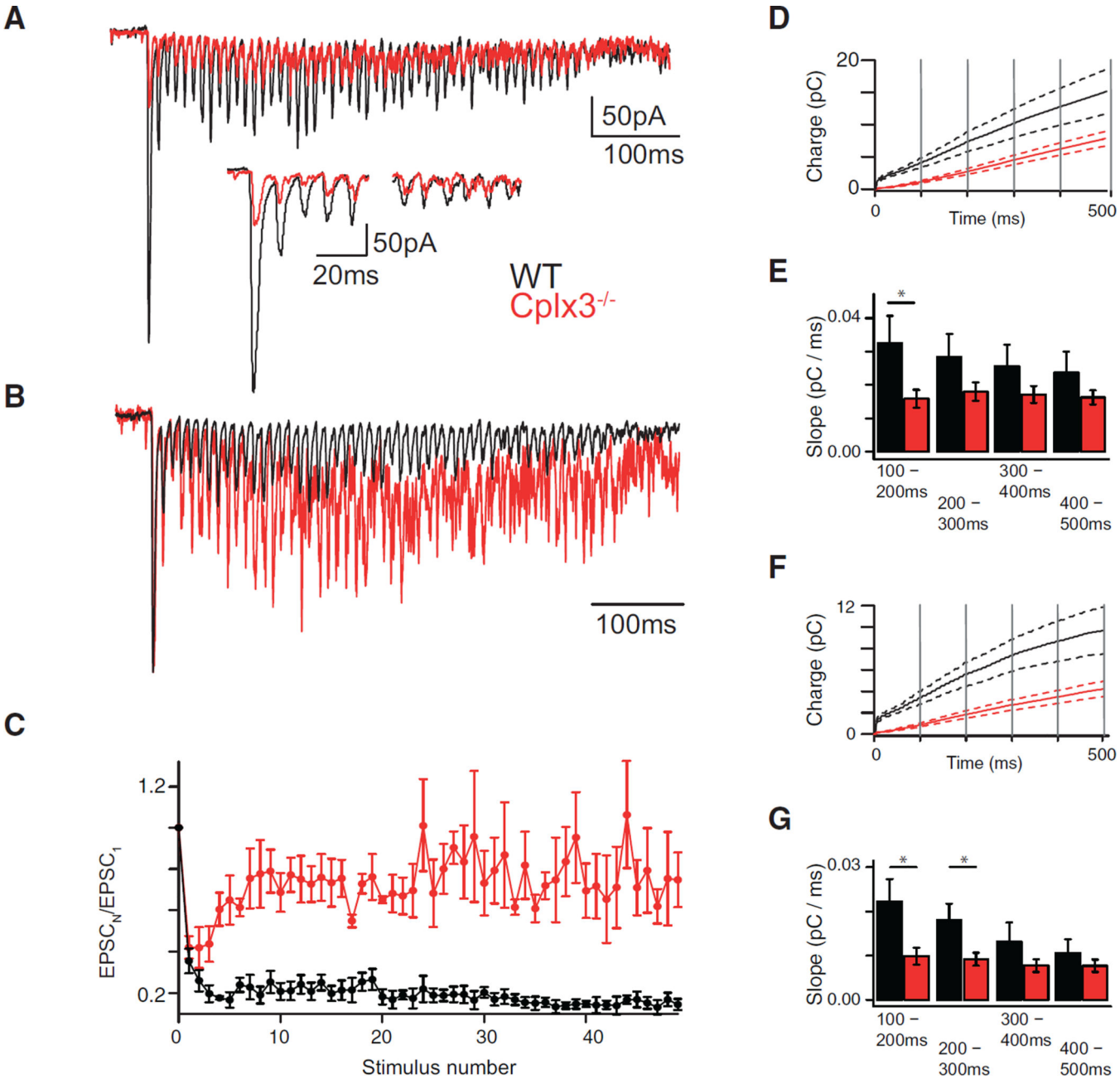

Figure 4. Use-Dependent Plasticity at RB → AII Synapses

(A and B) Depolarization train (3 ms to −10 mV at 100 Hz) evokes EPSCs in AIIs at WT (black) and Cplx3$^{-/-}$ (red) synapses. EPSC amplitudes depressed strongly during train (inset: first five and final five responses), but magnitude and timing of depression varied between WT and Cplx3$^{-/-}$, with Cplx3$^{-/-}$ showing recovery to a larger steady-state level (relative to the initial response, shown in B; EPSCs normalized to first response amplitude).

(C) Normalized amplitudes plotted against stimulus number.

(D and E) Integrated EPSCs divided into 100-ms bins (vertical gray lines). Solid lines indicate averages (WT, n = 5; Cplx3$^{-/-}$, n = 8), and dotted lines indicate SEM. Average slopes of each bin show initial recovery rate in WT synapses, but not Cplx3$^{-/-}$ synapses,

slowed with time (one-way repeated-measures ANOVA; WT versus Cplx3$^{-/-}$: $F(3, 12) = 6.971$, $p < 0.01$; versus $F(3, 21) = 1.337$, $p > 0.05$), with the most pronounced differences observed in the 100–200 ms window (WT versus Cplx3$^{-/-}$: 0.033 ± 0.008 versus 0.016 ± 0.003 pC/ms, $p = 0.039$, Student's t test).

(F and G) Same as in (D and E), but for phasic component alone (note smaller current integral values). WT data, but not Cplx3$^{-/-}$ data, were reduced in slope as sections advanced (one-way repeated-measures ANOVA; WT versus Cplx3$^{-/-}$: $F(3, 12) = 17.17$, $p < 0.001$; versus $F(3, 21) = 2.891$, $p > 0.05$), and post hoc analysis using Student's t test with a Bonferroni-Holm correction showed different slopes at 100–200 ms (WT versus Cplx3$^{-/-}$: 0.022 ± 0.005 versus 0.009 ± 0.002 pC/ms; $p = 0.04512$) and 200–300 ms (WT versus Cplx3$^{-/-}$: 0.018 ± 0.004 versus 0.002 ± 0.001 pC/ms; $p = 0.0459$). As in (E), recovery of phasic transmission is slowed more than that of transmission generally (including asynchronous release).

Data are presented as mean ± SEM. *$p < 0.05$.

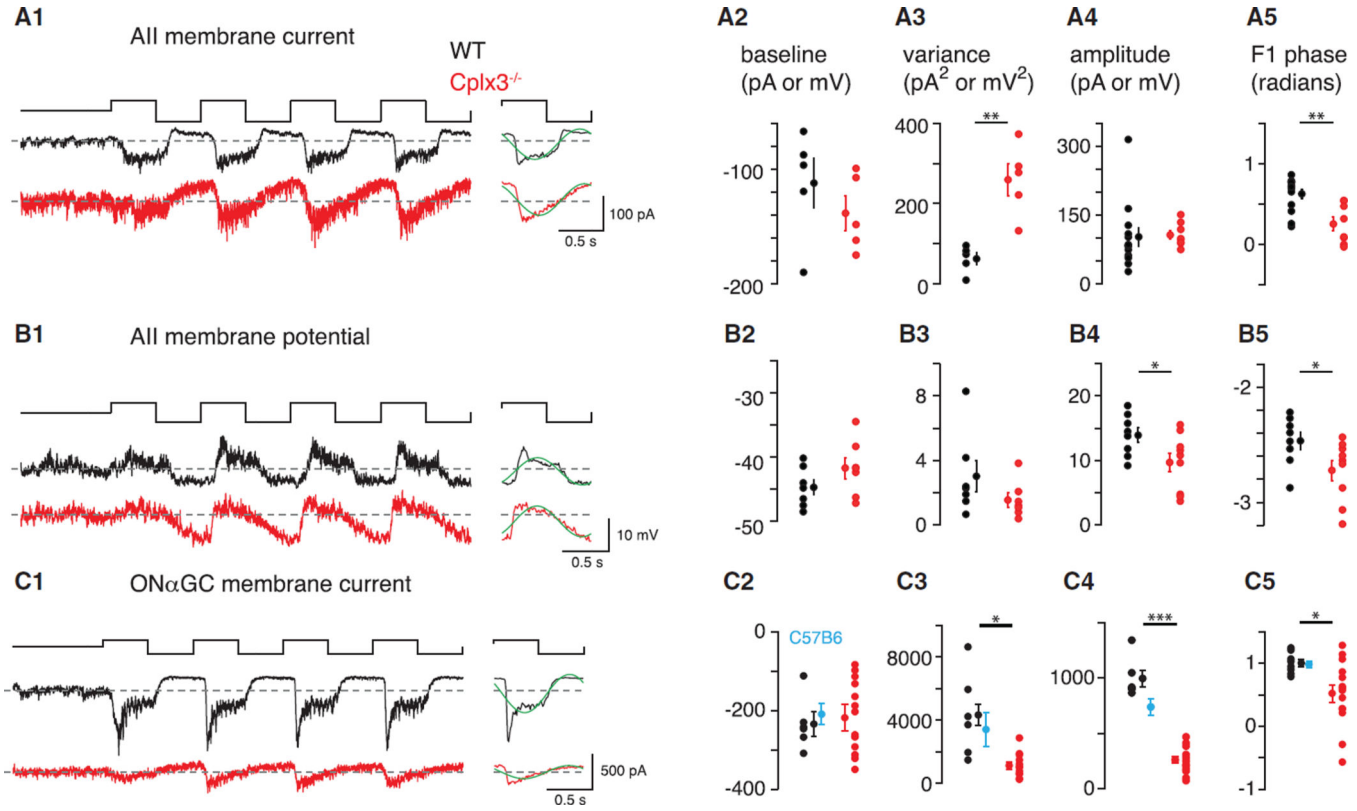

Figure 5. Cplx3$^{-/-}$ Slows and Attenuates Propagation of Rod-Mediated Signals through the RB → AII Circuit

(A1–A5) In (A1, left): I_{AII} (V_{HOLD} = −70 mV; 1 kHz sampling) during 100% contrast modulation (mean = 10 R*/rod/s) in Cplx3$^{-/-}$ and WT retinas. In (A1, right): average of last three cycles, binned at 100 Hz, with F1 Fourier component superimposed (green). (A2) Baseline current during mean luminance in both groups; mean ± SEM shown next to individual data points. (A3) I_{AII} variance measured over 2 s during mean luminance. (A4) Peak-to-peak amplitude of the binned, averaged response cycle (see A1, right). (A5) Phase of F1 Fourier component (see A1, right). (A2–A5) n = 5–13 in WT and 5–8 in Cplx3$^{-/-}$. (B1–B5) Same as in (A1–A5) for AII V_M (current-clamp recording). Average V_M measured over four cycles (B1) was depolarized significantly in the Cplx3$^{-/-}$ retina (−42.3 ± 1.6 versus −45.8 ± 1.1 mV in WT; $p < 0.05$, one-tailed Student's t test). (B2–B5) n = 7–8 in WT and 7–9 in Cplx3$^{-/-}$.

(C1–C5) Same as in (A1–A5) for I_{GC} (V_{HOLD} =−70 mV). (A2–A5) n = 6–8 in WT and 14 in Cplx3$^{-/-}$. Cplx3$^{+/+}$ WT littermate controls were similar to C57B6 WT controls (n = 6; cyan).

Data are presented as mean ± SEM. *$p < 0.05$; **$p < 0.002$; ***$p < 0.0001$.

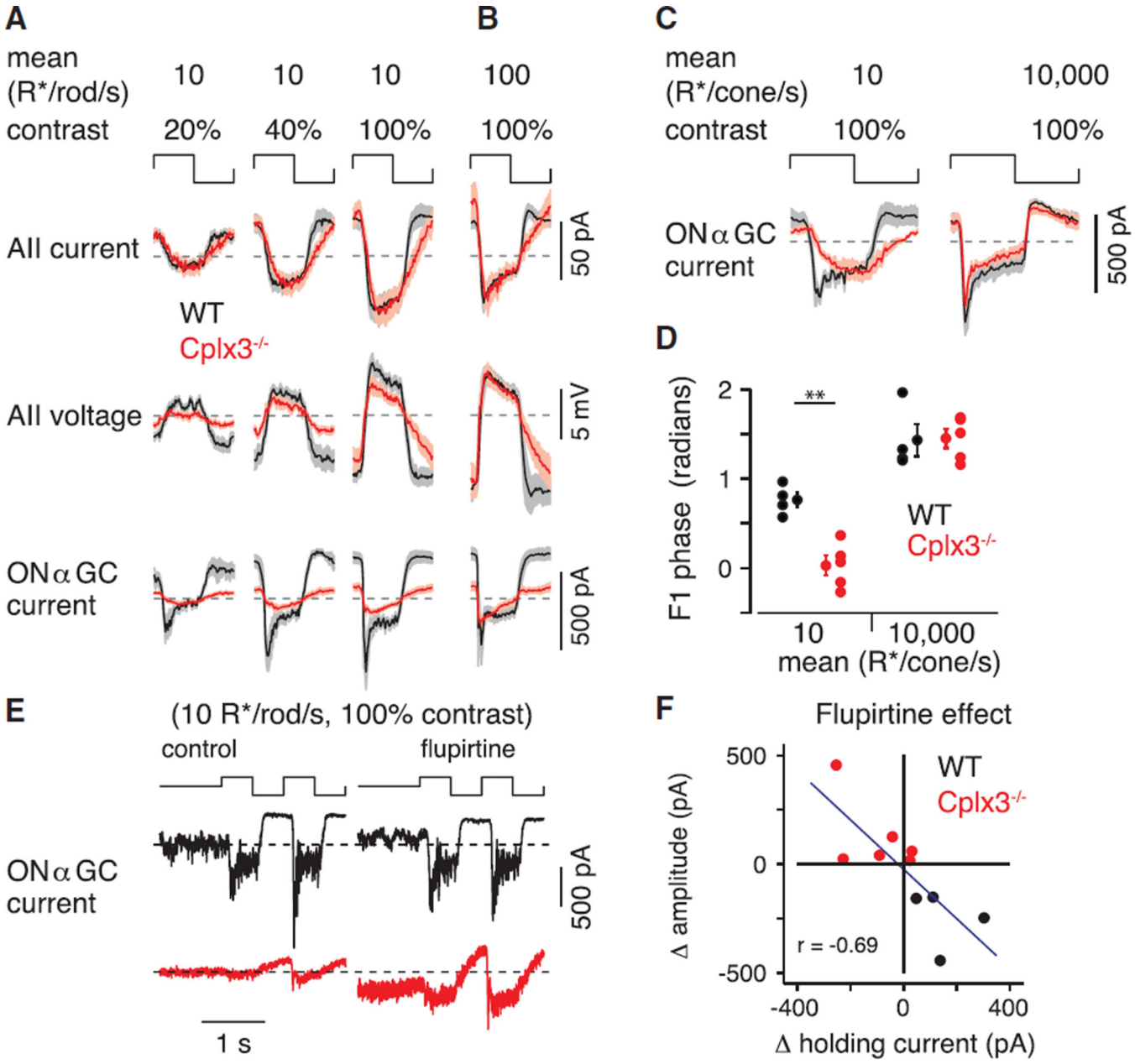

Figure 6. Cplx3$^{-/-}$ Affects RB but Not Cone-Pathway-Mediated Signaling

(A) Population average response cycles for multiple cell types and contrast levels. Traces indicate population mean for average response cycles (binned at 100 Hz) for each cell type and condition indicated (AII current: n = 13 WT, 8 Cplx3$^{-/-}$; AII voltage: n = 8 WT, 9 Cplx3$^{-/-}$; ONαGC: n = 6 WT, 14 Cplx3$^{-/-}$). Shading indicates ±SEM. Cplx3$^{-/-}$ causes phase delay in I_{AII}, primarily by delaying response at light offset. Cplx3$^{-/-}$ reduces amplitude in AII V_M and, more profoundly, amplitude of I_{GC}.

(B) The effect of Cplx3$^{-/-}$ extends to a brighter mean level that still activates primarily rods (compare to rightmost column in A) (AII current: n = 9 WT, 6 Cplx3$^{-/-}$; AII voltage: n = 8 WT, 8 Cplx3$^{-/-}$; ONαGC: n = 4 WT, 8 Cplx3$^{-/-}$).

(C) Responses to dim, bright UV light in ONαGC (n = 4 WT, 5 Cplx3$^{-/-}$). Response in dim light affected by Cplx3$^{-/-}$, as in (A) and (B), but a relatively normal response to bright light indicates intact CB pathways.

(D) Phase delay in I_{GC} evoked by dim, but not bright, UV stimulation of Cplx3$^{-/-}$ retinas (**$p < 0.002$).

(E) Example ONαGC responses (WT and Cplx3$^{-/-}$ retinas) to 100% contrast modulation (mean = 10 R*/rod/s) under baseline and flupirtine conditions.

(F) Effect of flupirtine (10 μM), relative to baseline, on holding current and peak-to-peak response amplitude to modulated contrast (n = 10): effect on holding current was negatively correlated with effect on response amplitude ($r = -0.69$, $p < 0.05$). Data are presented as mean ± SEM.

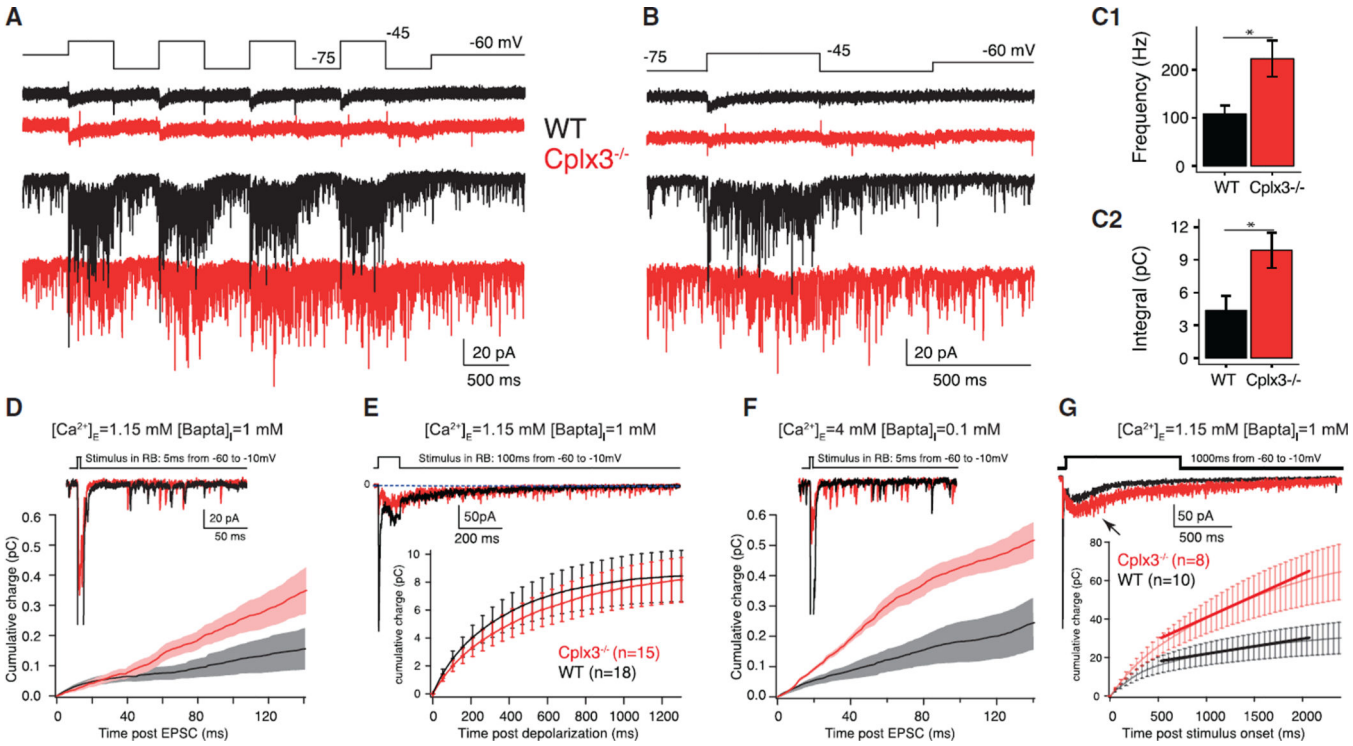

Figure 7. Asynchronous Release Evoked by Stimuli Mimicking the Presumed RB Response to Contrast

(A) Square wave stimulus (10 Hz) moved RB membrane potential above (−45 mV) and below (−75 mV) threshold for exocytosis and evoked I_{Ca} (top) and EPSCs (bottom) at WT (black; n = 5) and Cplx3$^{-/-}$ (red; n = 4) synapses.

(B) Last square wave cycle illustrated to demonstrate that release ceases more slowly upon hyperpolarization of Cplx3$^{-/-}$ RBs. Sustained currents during depolarization phases were statistically similar in WT and Cplx3$^{-/-}$: −20.2 ± 2.0 versus −19.5 ± 1.3 pA; p = 0.77.

(C1 and C2) Summary data illustrate elevated release frequency (C1; WT versus Cplx3$^{-/-}$: 108 ± 18 versus 223 ± 37 vesicles • s^{-1}; p = 0.04) and charge transfer (C2) at Cplx3$^{-/-}$ synapses during the hyperpolarizing phase. After the stimulus, release rate decayed back to baseline more slowly at Cplx3$^{-/-}$ synapses (WT versus Cplx3$^{-/-}$: t = 105 ± 58 versus 385 ± 78 ms; p = 0.022).

(D and E) Differences in asynchronous release between WT and Cplx3$^{-/-}$ are not observed when $[Ca^{2+}]_I$ is well buffered (WT, black; Cplx3$^{-/-}$, red). In (E, top): tonic charge transfer in WT (n = 17) and Cplx3$^{-/-}$ (n = 14) was statistically similar (WT versus Cplx3$^{-/-}$: 4.2 ± 0.8 versus 2.4 ± 0.5 pC; p > 0.05).

(F and G) Increasing $[Ca^{2+}]_I$ potentiates asynchronous release more in Cplx3$^{-/-}$ (WT, black; Cplx3$^{-/-}$, red). Integrated membrane currents plotted below the samples. In (G), the entire response was integrated and the first 400 ms after the end of the stimulus fitted with a line. Slopes were significantly different (WT = 22.7 ± 1.5; Cplx3$^{-/-}$ = 7.8 ± 0.9; p < 0.0001, Student's t test), revealing increased charge transfer after 1,000 ms stimulus. Note, too, appearance of delayed release component (arrow) after ~200 ms in (G). Delayed release was mildly slowed in onset and slightly larger in Cplx3$^{-/-}$ (WT versus Cplx3$^{-/-}$: 23.1 ± 5.4

versus 44.9 ± 8.1 pC; p = 0.036), but asynchronous release was enhanced significantly (WT versus Cplx3$^{-/-}$: 9,778 ± 619 versus 21,622 ± 1142 pC; p < 0.05).
Data points indicate mean ± SEM; Student's t test, *p < 0.05.